Magnetic fabrics in the basal ice of a surge-type glacier

Edward J. Fleming,[1,3] Harold Lovell,[2,3] Carl T. E. Stevenson,[1] Michael S. Petronis,[4] Douglas I. Benn,[3] Michael J. Hambrey,[5] and Ian J. Fairchild[1]

Received 25 March 2013; revised 6 September 2013; accepted 9 September 2013; published 31 October 2013.

[1] Anisotropy of magnetic susceptibility (AMS) has been shown to provide specific useful information regarding the kinematics of deformation within subglacially deformed sediments. Here we present results from debris-rich basal glacier ice to examine deformation associated with glacier motion. Basal ice samples were collected from Tunabreen, a polythermal surge-type glacier in Svalbard. The magnetic fabrics recorded show strong correlation with structures within the ice, such as sheath folds and macroscopic stretching lineations. Thermomagnetic, low-temperature susceptibility, varying field susceptibility, and isothermal remanent magnetism acquisition experiments reveal that the debris-rich basal ice samples have a susceptibility and anisotropy dominated by paramagnetic phases within the detrital sediment. Sediment grains entrained within the basal ice are inferred to have rotated into a preferential alignment during deformation associated with flow of the glacier. An up-glacier directed plunge of magnetic lineations and subtle deviation from bulk glacier flow at the margins highlight the importance of noncoaxial strain during surge propagation. The results suggest that AMS can be used as an ice petrofabric indicator for investigations of glacier deformation and interactions with the bed.

Citation: Fleming, E. J., H. Lovell, C. T. E. Stevenson, M. S. Petronis, D. I. Benn, M. J. Hambrey, and I. J. Fairchild (2013), Magnetic fabrics in the basal ice of a surge-type glacier, *J. Geophys. Res. Earth Surf.*, *118*, 2263–2278, doi:10.1002/jgrf.20144.

1. Introduction

[2] In this paper, we present a novel application of the anisotropy of magnetic susceptibility (AMS) technique to examine debris-rich basal ice. The flow of glacier ice can produce similar structures to those produced in ductile deformation within rocks [*Maltman et al*., 2000]. The analysis of these structures and smaller-scale ice fabrics can provide insight concerning the strain history and deformation of glacier ice, since ice crystals are anisotropic [*Castelnau et al*., 1998] and tend to develop a preferred orientation in response to strain.

[3] The most commonly used method to examine fabrics within glacier ice is the analysis of *c* axis crystallographic orientations of ice crystals in thin section [e.g., *Bader*, 1951; *Rigsby*, 1958] . This has been particularly useful in understanding how ice deforms under stress [*Wilson*, 2000; *Wilson and Sim*, 2002]. More recently, the development of automated techniques has introduced greater speed and objectivity [*Wilen et al*., 2003]. However, *Tison and Lorrain* [1987] showed that glacier ice can recrystallize over quite short timescales, so the final measured fabric may not represent the cumulative strain but rather a more recent recrystallization event.

[4] Fabric analysis involving the measurement of the AMS [*Tarling and Hrouda*, 1993] has provided considerable insight into depositional [e.g., *Ellwood and Ledbetter*, 1977; *Hooyer et al*., 2008; *Lagroix and Banerjee*, 2002] and deformation histories [e.g., *Borradaile and Jackson*, 2004; *Cifelli et al*., 2009; *Parés et al*., 1999] of rock and sediment. In recent years, the technique has provided interesting new information about various aspects of glaciology including facilitating the interpretation of bed deformation [*Hooyer et al*., 2008; *Iverson et al*., 2008], glacier flow direction [*Shumway and Iverson*, 2009; *Thomason and Iverson*, 2009], and glaciotectonic history [*Fleming et al*., 2013] of deformed glacial sediment. Despite the links between styles of deformation seen in glaciers to those of rocks and sediment, there is (to our knowledge) no published research on the AMS of glacier ice.

[5] Glacier ice formed by the firnification of snow, often termed englacial ice [e.g., *Hubbard et al*., 2000], is dominated by H_2O and is therefore diamagnetic (negative susceptibility) [*Lanci et al*., 2001]. While the AMS of rocks dominated by diamagnetic minerals has been used to investigate structural deformation [e.g., *Borradaile et al*., 2012; *de Wall et al*., 2000; *Owens and Rutter*, 1978], compared to that with ferromagnetic and paramagnetic dominated minerals, their relationship to strain is not as well understood, and research into the

[1]School of Geography, Earth and Environmental Sciences, University of Birmingham, Birmingham, UK.
[2]School of Geography, Queen Mary University of London, London, UK.
[3]Department of Geology, University Centre in Svalbard (UNIS), Longyearbyen, Norway.
[4]Natural Resource Management, New Mexico Highlands University, Las Vegas, New Mexico, USA.
[5]Institute of Geography and Earth Sciences, Aberystwyth University, Aberystwyth, UK.

Corresponding author: E. J. Fleming, School of Geography, Earth and Environmental Sciences, University of Birmingham, Birmingham B15 2TT, UK. (ejf011@bham.ac.uk)

2169-9003/13/10.1002/jgrf.20144

magnetic anisotropy of H_2O ice has not been carried out. Unlike englacial ice, there is a zone of ice at the base of glaciers and ice sheets which exhibits a distinct set of physical and chemical properties formed by processes operating at the bed, commonly referred to as basal ice [*Hubbard et al*., 2009; *Hubbard and Sharp*, 1989; *Knight*, 1997]. This ice is thought to have predominantly formed through processes including adfreezing, regelation, and hydraulic supercooling [*Cook et al*., 2006; *Hubbard*, 1991; *Hubbard and Sharp*, 1993] at the base of glaciers and ice sheets and, as such, has the ability to incorporate significant amounts of detrital minerals or subglacial sediment en masse [*Hambrey et al*., 2005]. Depending on the composition of the source material, this detrital material is expected to contain paramagnetic and ferromagnetic grains that will overwhelm the diamagnetic signal and create fabrics which retain more of a signal related to ice deformation. The basal ice of glaciers and ice sheets therefore represents a suitable candidate for potential AMS investigations.

[6] Glacier ice flows in response to gravitational forces acting on a sloping ice body; however, this flow is resisted by friction at the bed and lateral margins. Being located in the zone between the bed and the bulk of the glacier ice, basal ice is shown to be strongly affected by glacial motion and is commonly highly deformed [*Larsen et al*., 2010; *Samyn et al*., 2010; *Souchez et al*., 2000]. As such, a variety of structures are produced reflecting compression, extension, or simple shear, depending on the flow regime of the glacier. Basal ice commonly exhibits a strong ice-crystal *c* axis fabric [*Samyn et al*., 2008]. As a result, one may expect fabrics associated with such deformation, as well as being recorded in the diamagnetic ice, to be preserved through a preferred orientation of grains within the detrital sediment. Therefore, in theory, an AMS fabric should develop within the detrital component of basal ice that reflects the cumulative strain history.

[7] In this study, we apply the AMS technique to basal ice exposed at the margin of a surge-type tidewater glacier in Svalbard. The aims of this study are to (i) characterize the AMS fabric by determining the orientation and degree of alignment and shape of the susceptibility ellipsoid. Also, since different minerals can produce vastly different fabric characteristics (e.g., inverse fabric in single domain magnetite) [*Ferré*, 2002], the magnetic mineralogy of the ice is investigated through rock magnetic experiments. (ii) Determine the relationship of the fabric to other visible strain indicators within the ice at both outcrop scale and through the analysis of aerial photographs. (iii) Examine the relationship of the fabric to the recent surge activity of the glacier. Through these investigations, the potential of the AMS technique for the analysis of basal ice is evaluated and future areas in which the technique could be applied are suggested.

2. AMS Theory

[8] AMS is one of a group of techniques that can be used to measure the physical arrangement of particles and minerals (petrofabric) in rock or sediment. It works on the principle that when subjected to an external magnetic field, an induced magnetism is generated in rock or sediment that is dependent on the magnetic susceptibility, (K) represented by the equation $M = KH$, where M is the induced magnetization, H is the applied field, and K is the susceptibility measured in SI units[*Tarling and Hrouda*, 1993].

[9] Susceptibility is essentially a measure of the Fe content in a sample but is also controlled by the alignment, distribution, or crystalline orientation of these mineral grains and so is anisotropic. In this way, the magnetic fabric normally represents the petrofabric of the rock or sediment, thus providing information on its formation/deformation. AMS can be used to accurately determine fabric in three dimensions and is best visualized as an ellipsoid with a long (K_1), intermediate, (K_2) and minimum (K_3) axis. While the AMS records the petrofabric of a rock, it is an oversimplification to assume that K_1 reflects the mean orientation of the long axis of grains. This is because mineral composition and grain size can greatly affect how it behaves in response to an external magnetic field, and as such, the magnetic mineralogy needs to be explored before reliable fabric interpretations can be made.

[10] Most minerals forming a rock or sediment can be defined by three magnetic behaviors: ferromagnetic, paramagnetic, and diamagnetic. Ferromagnetic minerals (which include ferrimagnetic sensu strictu minerals, e.g., magnetite) have a strongly proportional relationship between M (induced magnetism) and H (strength of applied field), with a maximum value of M. These grains retain their magnetism when subjected to a high magnetic field, and therefore carry a remanent magnetism (as used in paleomagnetic analysis). Ferromagnetic minerals have very high susceptibilities (e.g., 1500×10^{-3} for magnetite) and will dominate the fabric even if present in very small concentrations. They can easily be identified based on their thermomagnetic properties as they have a structure that limits thermal disruption up to the Curie temperature, after which grains behave paramagnetically [*Dunlop and Özdemir*, 1997]. In contrast, paramagnetic minerals have a proportional, nonpermanent relationship between M and H. Paramagnetism is exhibited in silicate minerals that contain Fe in the crystal lattice (e.g., biotite and chlorite). An important property in the detection of paramagnetism is that susceptibility decreases with increase temperature according to the Curie-Weiss law. Finally, diamagnetic minerals (e.g., quartz and calcite) have a slight negative response to increasing H. Diamagnetism is present in all rocks but has very weak, negative susceptibilities (-1×10^{-4}) [*Tarling and Hrouda*, 1993] and is normally overshadowed by even small amounts of paramagnetic or ferromagnetic grains.

[11] Minerals can be classified as having shape, crystalline, or distribution anisotropies. Shape anisotropy is common in ferromagnetic grains (e.g., magnetite) and occurs when the induced magnetization is preferentially orientated along the axis of the grain. Crystalline anisotropy is common in paramagnetic minerals (e.g., chlorite) and occurs where the induced magnetization is dependent on the orientation of the crystal lattices within the mineral (commonly with K_3 perpendicular to the basal plane). In many examples, the fabrics produced from shape and crystallographic anisotropy are directly compatible [e.g., *Cifelli et al*., 2009]. This is because paramagnetic minerals (e.g., chlorite) tend to break preferentially along basal planes and under extensional strain, these basal planes have been shown to girdle about an axis parallel to extension, creating what is effectively an intersection lineation [*Cifelli et al*., 2005]. Distribution anisotropy can play a role if ferromagnetic grains are not randomly distributed through the matrix due to magnetostatic interactions [*Hargraves et al*., 1991].

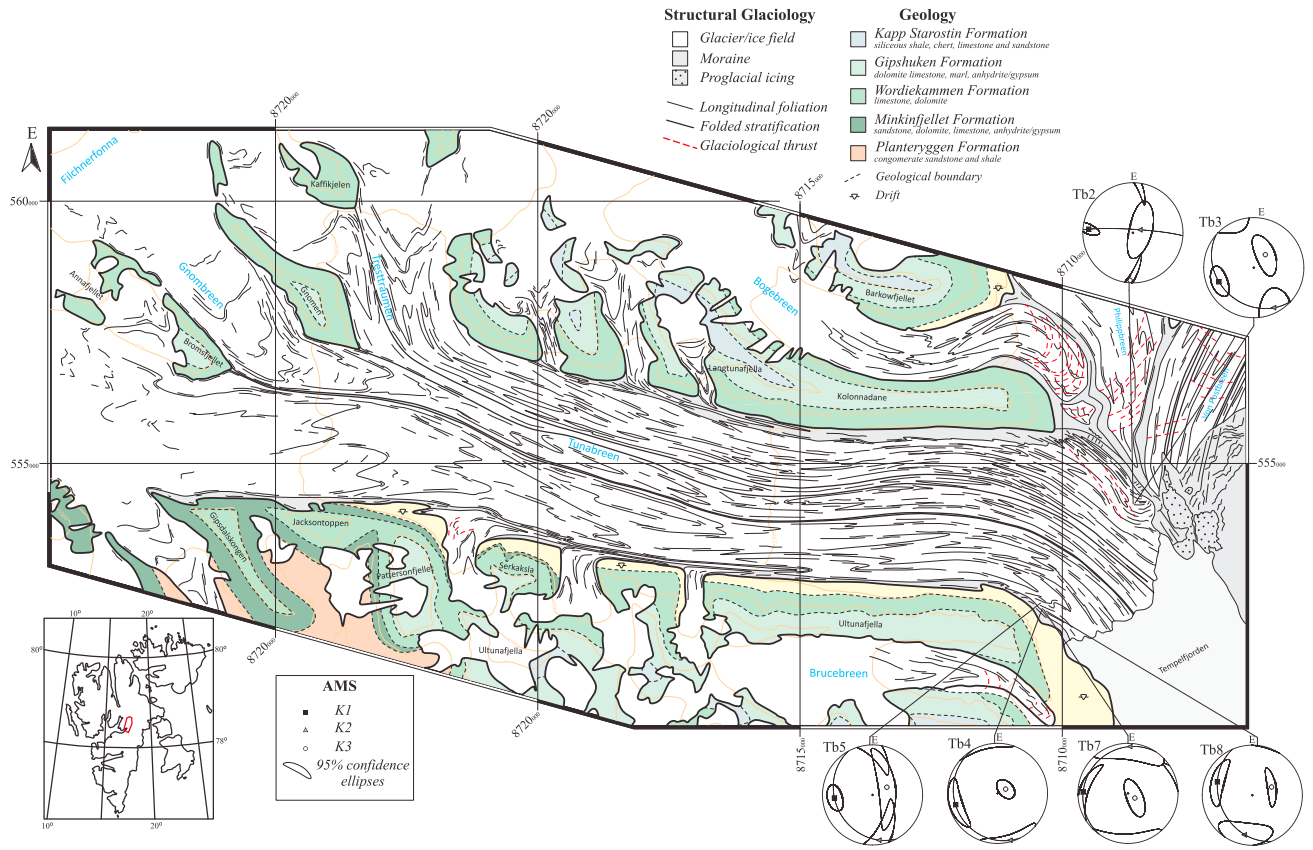

Figure 1. Geological map of Tunabreen and surrounding area, with glaciological structures and magnetic fabric results. Geology redrawn after *Dallmann et al*. [2009, 2011]. Glaciological structures drawn from aerial photographs dated July 2004. AMS results are plotted onto lower hemisphere, equal-area stereographic projections showing the mean susceptibility ellipsoids with the 95% confidence ellipsoids and the magnetic foliation (great circles) derived from the K_3 orientation. Inset map shows location of study area within Svalbard.

[12] In addition to this, grain size can play an important role in the response of minerals in rock or sediment to an external magnetic field. Some minerals (e.g., magnetite), when present in sizes below 0.03 µm, will exhibit single domain behavior where susceptibility axes can switch creating "inverse" fabrics [*Ferré*, 2002]. As such, proper determination of the magnetic mineralogy is vital (see section 4 for discussions of methods used) to enable reliable conclusions to be drawn.

[13] AMS can characterize and quantify very weak or subtle mineral fabrics and has been widely used in geology as a means for investigating the processes involved in the formation of rocks and sediments [see references in *Tarling and Hrouda*, 1993]. It is an important tool in understanding how a material deforms in response to tectonic deformation as stress acting on the sediment can cause grains to rotate resulting in a preferential alignment. In glacial sedimentology, the AMS of subglacial sediments has the ability to reveal subtle fabrics relating to ice deformation [*Eyles et al*., 1987; *Fleming et al*., 2013; *Gentoso et al*., 2012; *Shumway and Iverson*, 2009; *Thomason and Iverson*, 2009]. As well as various field-based applications, the technique has been verified through laboratory testing [*Hooyer et al*., 2008; *Iverson et al*., 2008]. In these experiments, tills were sheared under conditions thought to be operating at the bed. Microshears were seen to develop that facilitate the rotation of grains into the shear plane where they remain. This evidence was used in support of the idea of March-type rotation [*March*, 1932], where particles can role continuously in a viscous shearing medium [*Thomason and Iverson*, 2006]. Basal ice generally lies immediately above subglacial sediment and plays an important role in its formation through melt-out or lodgment [*Benn and Evans*, 2010]. However, the way that sediment particles within the ice respond to strain is not well understood. The application of AMS to basal ice offers excellent opportunity for some of these ideas to be investigated.

3. Glaciological and Geological Setting

[14] Tunabreen is a 33 km long tidewater glacier located in central Svalbard (Figure 1). The glacier drains from the Filchnerfonna and Lomonosovfonna ice caps and flows into Tempelfjorden. The surrounding bedrock geology consists of undeformed gently dipping Permian and Carboniferous sediments composed of conglomerate, sandstone, and shale of the Billefjorden Group. In turn, these are overlain by locally fossiliferous sandstones, carbonates, shales, and cherts of the Dickson Land Subgroup [*Cutbill and Challinor*, 1965]. These strata were mostly deposited on a stable carbonate platform under shallow marine conditions [*Harland et al*., 1997].

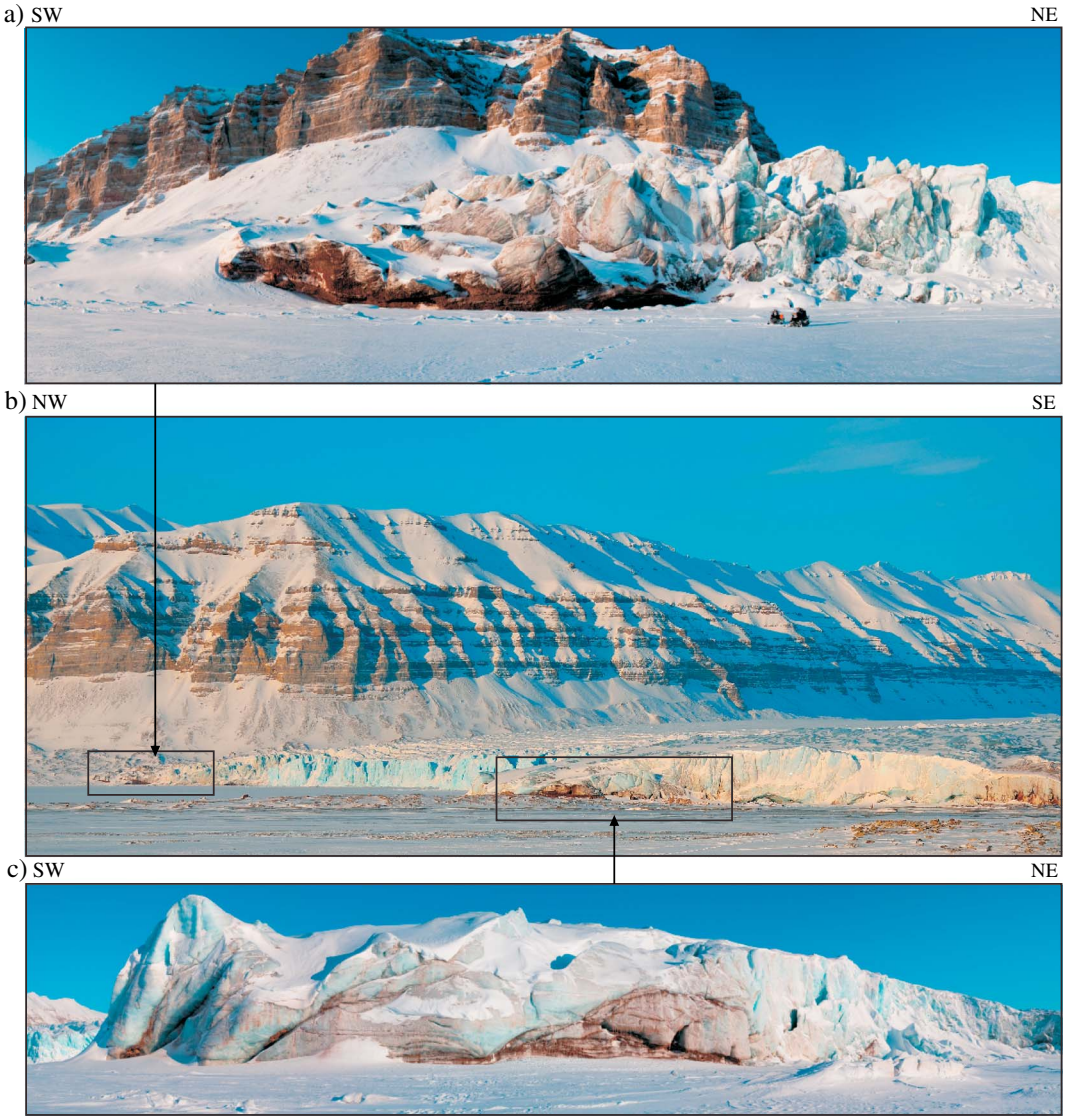

Figure 2. Field photographs of Tunabreen and the sections sampled. (a) NW section at the lateral margin of Tunabreen. Blue ice in the right of the photograph represents englacial ice while the basal ice is shown by the darker brown horizon in the center (snowmobile in foreground = 1 m). Height of section = 15 m. (b) Photograph showing the locations of the NW and SE sections taken from the lateral moraine of Von Postbreen. (c) SE section showing englacial ice (blue) overlying basal ice (brown and banded). Height of section = 30 m.

[15] Radio echo-sounding records indicate that the glacier is polythermal [*Bamber*, 1987]. Tunabreen is a surge-type glacier and is the only one in Svalbard known to have surged 3 times, producing a consistent return period of approximately 40 years. Tunabreen last surged in 2003–2005, during which the terminus advanced by up to 2 km into Tempelfjorden. Since surge termination, Tunabreen has calved back to its present-day position, revealing spectacular and easily accessible exposures of the basal zone of the glacier at the lateral margins, including the glacier bed interface. There are three dominant ice facies within the exposures: a banded debris-rich facies composed of alternating bands or laminae (1–10 mm thick) of ice-containing diamicton and clean bubble-free ice, a solid debris-rich facies composed of diamicton with some stratification (hereafter referred to as "banded facies" and "solid facies," respectively) [after *Hubbard et al.*, 2009], and a clean, bubbly facies (hereafter termed "englacial facies") [after *Hubbard et al.*, 2000].

[16] The flow regimes of Tunabreen are indicated through structures exposed at the surface of the glacier (Figure 1). Ice stratification and longitudinal foliation (utilizing glaciological terminology of *Hambrey and Lawson* [2000]) are clearly seen in aerial photographs. This stratification, which originates in an orientation defined by the margins of the flow boundaries in the accumulation zone, becomes folded as the ice flows. Fold tightness increases down-glacier, evolving to isoclinal toward the terminus. Fold limbs are rotated

Table 1. Mean Site AMS Data (See Section 3 for Calculation)[a]

Site	N	K_m	K_1	K_1 95% Error	K_2	K_2 95% Error	K_3	K_3 95% Error	L	F	P_j	T
TB2	6	9.04E-06	**4/12.5**	*22/6*	**160/76**	49/19	**273/6**	49/4	1.018	1.052	1.077	-0.046
TB3	13	2.28E-05	**338/26**	*36/21*	**243/11**	36/21	**132/62**	35/16	1.017	1.009	1.027	-0.303
TB4	7	1.28E-05	**345/15**	*34/13*	**254/3**	35/12	**152/75**	18/12	1.022	1.035	1.058	0.227
TB5	12	2.37E-05	**355/25**	*19/14*	**261/9**	71/13	**152/63**	71/14	1.076	1.024	1.107	-0.512
TB7	11	1.87E-05	**2/11**	*46/9*	**93/7**	46/26	**214/77**	33/13	1.012	1.025	1.038	0.335
TB8	12	1.89E-05	**21/26**	*35/12*	**280/21**	38/22	**157/56**	31/7	1.037	1.028	1.066	-0.142

[a]N = Number of Samples; K_m = Mean Susceptibility; K_1, K_2, K_3 = Orientations (Declination and Inclination) of the Principal Susceptibility Axes with 95% Confidence Ellipses; L = Lineation ($L = K_1/K_2$); F = Foliation ($F = k_2/k_3$); P_j = Anisotropy Degree; T = Shape Parameter.

parallel to the glacier margins and axial planes lie parallel to glacier flow direction, creating flow-parallel structures trending at 5°, which is commonly referred to as longitudinal foliation [*Hambrey and Lawson*, 2000], a phenomenon well known from Svalbard glaciers [e.g., *Hambrey and Glasser*, 2003; *Hambrey et al*., 2005].

[17] At the height of the most recent surge in 2004, almost the entire length of Tunabreen exhibited intense surface crevassing. Transverse crevasses dominated the pattern, forming perpendicular to the longitudinal foliation and glacier flow direction. Tunabreen has a tidewater margin and is dominated by a strong extensional flow regime during surges, a characteristic often seen in other Svalbard tidewater surge-type glaciers [cf., *Hodgkins and Dowdeswell*, 1994; *Murray et al*., 2003] without the compressional deformation commonly exhibited at the terminus of land-terminating Svalbard glaciers [*Hambrey et al*., 2005]. However, toward the terminus, the eastern margin of Tunabreen reaches a confluence with the neighboring Bogebreen, Phillippbreen, and Von Postbreen. Here a component of oblique compressional deformation is seen through the presence of structures that crop out at the surface which truncate foliation and crevasse patterns, interpreted as thrusts (Figure 1). This, combined with a changing coastal morphology, results in the deviation of flow at this location from a predominantly southward direction into a SSW direction.

4. Methods

[18] Two sections were analyzed at the lateral margins of Tunabreen, hereafter referred to as the northwest (NW) and southeast (SE) sections (Figure 2). Six sites were chosen from the banded basal ice facies, covering both lateral and vertical changes. In order to increase the chances of the acquisition of reliable fabrics, sites were chosen where the sediment concentration was greater than 10% by volume. Cores were collected during April 2011, using a portable rock drill with a 2.5 cm diameter, nonmagnetic, diamond-tipped drill bit, and orientated using a Brunton compass by scratching a fiducial mark on to the side of the core. Cores were subsequently transported to a cold room (at −20°C) at the University Centre in Svalbard and cut using a nonmagnetic, diamond-tipped circular rock saw into 21 mm sections, making one to two samples from each core. Sedimentological and structural data were collected in the field using standard procedures [cf. *Evans and Benn*, 2004]. Structural data from the measurement of mineral lineations were collected in March 2012.

[19] The AMS was measured using an AGICO KLY-3 Kappabridge operating at 875 Hz with a 300 A/m applied field at the University of Birmingham and an AGICO MFK-1A Kappabridge operating at 976 Hz with a 200 A/m applied field at New Mexico Highlands University. In total, 71 samples were analyzed with an average of 10 subsamples per site. The following parameters were used to evaluate the susceptibility ellipsoid [cf. *Tarling and Hrouda*, 1993]. The mean susceptibility (K_{mean}) is given by

$$K_{\text{mean}} = \frac{K_1 + K_2 + K_3}{3},$$

where $(K_1 > K_2 > K_3)$ are the principal susceptibilities (SI units). The shape of the ellipsoid can be characterized using lineation (L) and foliation (F) parameters [*Khan*, 1962] and are calculated as

$$L = \frac{(K_1 - K_2)}{K_{\text{mean}}}$$

and

$$F = \frac{(K_2 - K_3)}{K_{\text{mean}}}.$$

[20] Also used are the corrected anisotropy degree (P_j), to determine the strength of the fabric, and the shape parameter (T), to define the shape of the susceptibility ellipsoid [*Jelínek*, 1981], which respectively are

$$P_j = \exp\left(\sqrt{2\left[\left(\ln\left(\frac{K_1}{K_3}\right)\right)^2 + \left(\ln\left(\frac{K_1}{K}\right)\right)\right]}\right)$$

and

$$T = \left[\frac{2\ln\frac{K_2}{K_3}}{\ln\frac{K_1}{K_3}}\right] - 1.$$

[21] Because of the low susceptibility of the samples, careful cleaning and calibration of the sample holder were undertaken between each site, as even small amounts of ferromagnetic or paramagnetic dust may swamp the susceptibility signal of the samples [*Borradaile et al*., 2012]. In spite of the Kappabridge being sensitive to 0.5×10^{-8} SI with an accuracy of 0.1%, the anisotropy values near zero can be anomalously high [*Biedermann et al*., 2013; *Hrouda and Kapička*, 1986; *Rochette*, 1987]. Although this is not thought to affect fabric orientations [*Callot et al*., 2010; *Hrouda*, 2004], its effect can cause problems when calculating the

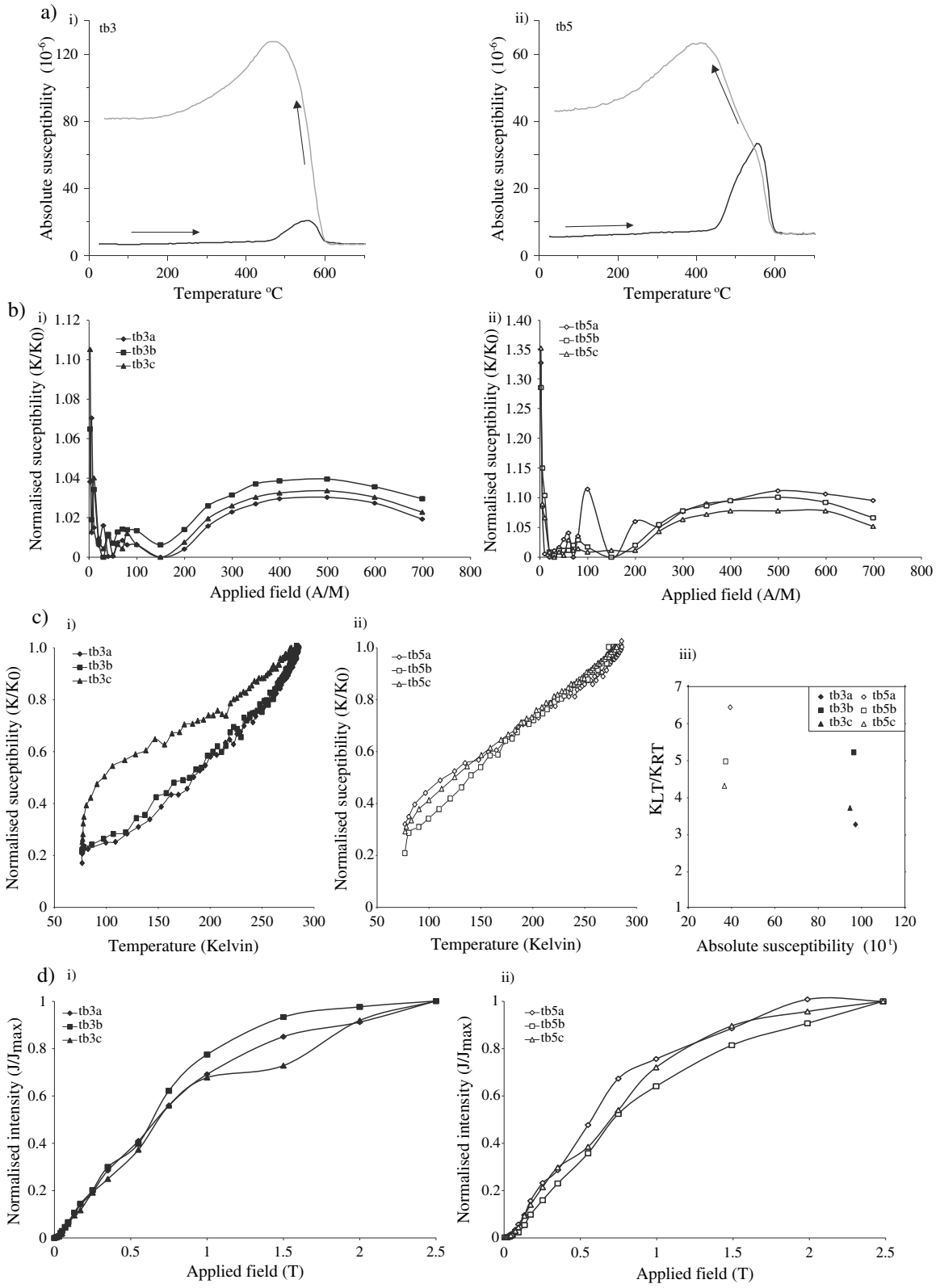

Figure 3. Rock magnetic experiments. (a) Low-field susceptibility (K) versus temperature curves for (i) NW and (ii) SE sections. In each case, the heating curve is black and the cooling curve is gray. (b) Low-field susceptibility versus applied field (A/M) curves normalized to the lowest susceptibility value (K/K_0) for (i) NW and (ii) SE sections. (c) The normalized reciprocal (K/K_0) susceptibility versus temperature for (i) NW and (ii) SE sections and (iii) the ratio of the susceptibility at the lowest temperature to the susceptibility at room temperature (K_{LT}/K_{RT}), plotted against magnetic susceptibility. (d) IRM experiments showing variation in normalized magnetic intensity (J/J_{max}) with applied field (T) for (i) NW and (ii) SE sections.

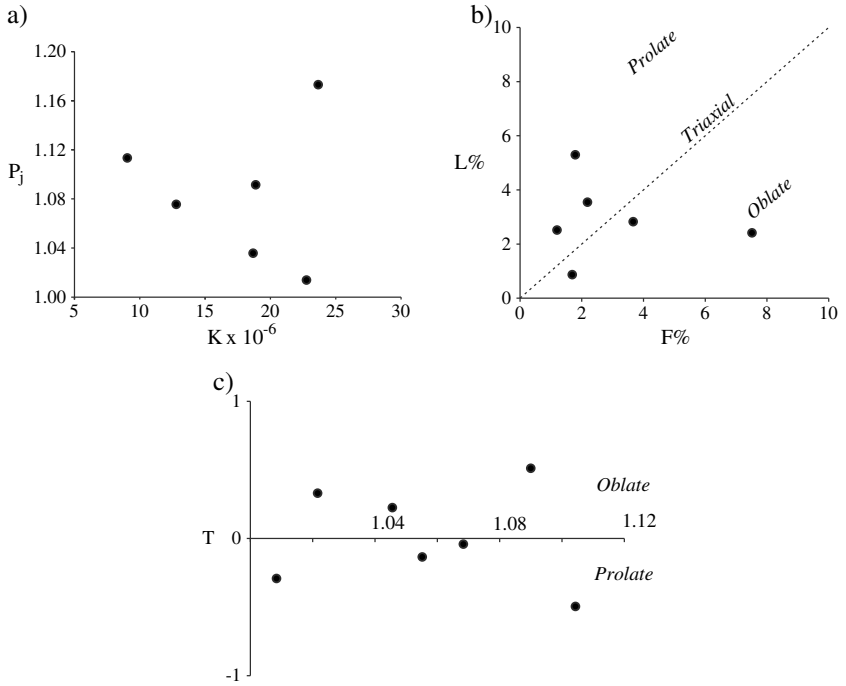

Figure 4. Variation of AMS parameters for all sites. (a) Anisotropy parameter (P_j) versus susceptibility (K). (b) L % versus F % (magnetic lineation versus magnetic foliation). (c) Shape parameter (T) versus anisotropy parameter (P_j).

anisotropy parameters, and as such, any subsamples with susceptibilities in the range of −5 μSI to 5 μSI were discounted, as recommended by *Hrouda* [2004].

[22] In all AMS investigations, determination of the magnetic mineralogy is of importance because of the different fabric characteristics which can be produced by different minerals. The detrital component, typically 10–40% volume of sample volume, was extracted from the diamagnetic H_2O by sublimation, and investigations of the magnetic mineralogy were conducted at New Mexico Highlands University. The variation of low-field magnetic susceptibility with temperature and field strength was conducted on an AGICO MFK-1A Kappabridge with a CS4 high-temperature susceptibility attachment. Thermomagnetic experiments were conducted for six samples from two sites measuring variations of magnetic susceptibility on heating at a 6°C interval from room temperature (20°C) to 700°C. Low-temperature susceptibility experiments were conducted on all sites using an in-house cryostat system coupled with the Kappabridge. The samples were cooled to 77 K in liquid nitrogen, and the bulk susceptibility measured every 18 s during warming to room temperature. The low-field variation of AC susceptibly was measured in the following fields: 5, 10, 20, 30, 40, 50, 60, 70, 80, 100, 150, 200, 250, 300, 350, 400, 500, 600, and 700 A/M following the procedure of *Hrouda et al.* [2006]. In addition, the ferromagnetic fraction of six samples was analyzed through the acquisition of Isothermal Remanent Magnetization (IRM) experiments (i.e., partial hysteresis loops), first by demagnetizing the sample in an alternating field (AF) to remove the natural remanent magnetism (NRM), followed by applying an external field at progressive stronger fields up to a peak of 2.5 tesla (T) field. This experiment was measured on an AGICO JR6-A dual-speed spinner magnetometer in a magnetically shielded room that attenuates Earth's field to less than 0.1%.

5. Results

5.1. Magnetic Mineralogy

[23] The mean susceptibility (K_{mean}) of the samples ranges from 9 to 23 μSI (average 20 μSI, Table 1), well within the paramagnetic realm [*Tarling and Hrouda*, 1993]. The magnetic susceptibility of the samples in which the detrital sediment was separated from the ice are 96 μSI for TB3 and 38 μSI for TB5, reflecting the absence of diamagnetic H_2O.

[24] Low-temperature susceptibility measurements (Figure 3c) can be used to distinguish between the contribution of paramagnetic from ferromagnetic phases, since antiferromagnetic, diamagnetic, and most ferromagnetic minerals have a temperature-independent susceptibility in the 77 to 295 K temperature range [*Richter and van der Pluijm*, 1994]. The curves show good Curie-Weiss temperature dependence, where susceptibility decreases with increasing temperature [*Nagata*, 1961]. The ratio of low-temperature/room temperature versus the mean value of room temperature susceptibility are plotted (Figure 3c) and the ratio of all samples is above 3.2, indicating a substantial paramagnetic component to the low-field AMS.

[25] The variation of low-field susceptibility with temperatures from 20 to 700°C (Figure 3b) shows a decreasing susceptibility with increase of temperature on some curves within the range of 20 to 250°C following Curie-Weiss behavior (Figure 3bi), whereas others show an independent or slight increase in susceptibility within this range (Figure 3bii). Above 250°C, all samples show an increase in susceptibility

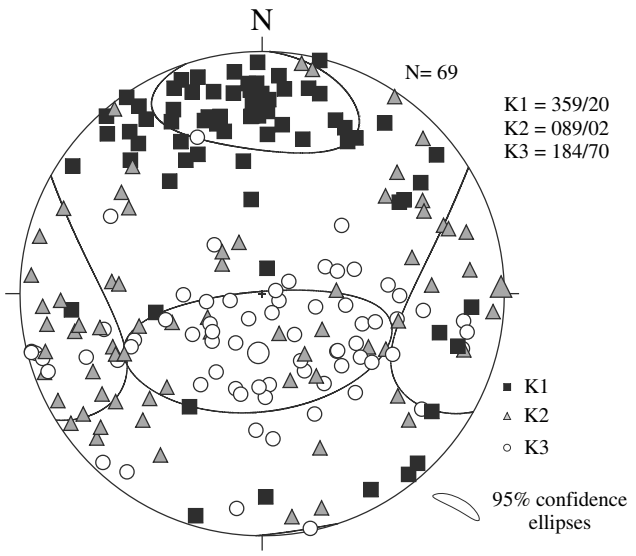

Figure 5. Stereographic projection of AMS results from all samples showing K_1 (black squares), K_2 (gray triangles), and K_3 (white circles) with 95% confidence ellipses. Refer to section 3 for derivation of anisotropy parameters.

with increasing temperature and exhibit strong peaks at 560°C, presumably indicating either the growth of new ferromagnetic phases on heating, or the "Hopkinson peak" owing to a minor amount of Fe-Ti oxide present within the sample.

[26] The variation of field strength with susceptibility can also be used to provide constraints on the magnetic mineralogy (Figure 3c). This experiment works on the principle that diamagnetic and paramagnetic minerals exhibit a linear relationship between magnetization and the magnetization field, whereas the susceptibility of some ferromagnetic minerals exhibit a strong field-dependent susceptibility [*Hrouda et al.*, 2006]. Nonsystematic behavior is seen in all samples in the 0 to 200 A/M range reflecting the high error margin in the measurement of susceptibility at these frequencies in low-susceptibility samples. However, above 200 A/M, all samples show a field-dependent susceptibility, which increases up to 500 A/M before decreasing. This presumably represents a minor contribution to the susceptibility by a ferromagnetic component.

[27] This ferromagnetic component is investigated further through the acquisition of IRM (Figure 3d). This works on the principle that the coercivity of a mineral varies with composition and grain size [*Dunlop and Özdemir*, 1997].

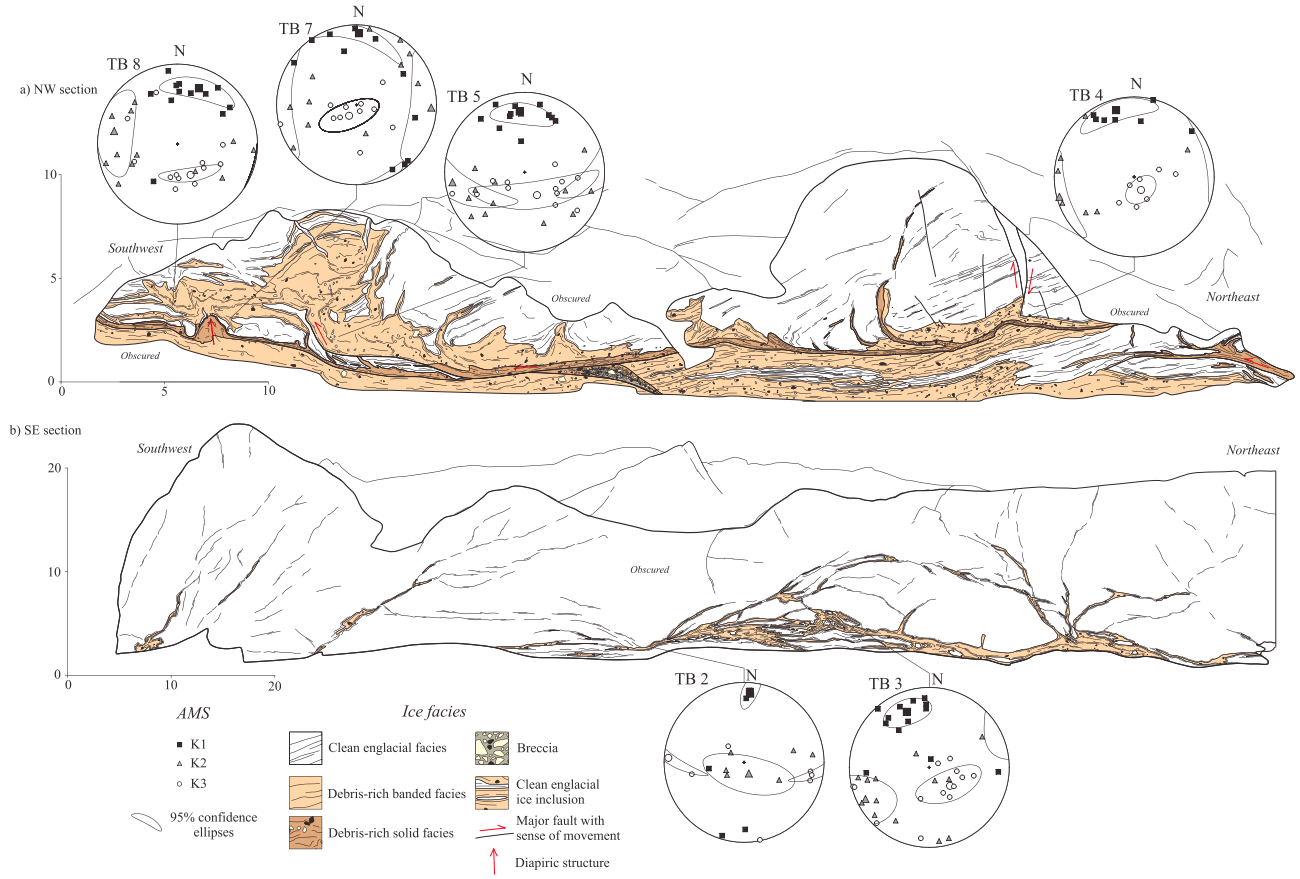

Figure 6. Two-dimensional section logs of (a) NW section and (b) SE section (no vertical exaggeration), with magnetic fabrics for all sites showing the three mean principal susceptibility axes plotted on to lower hemisphere stereographic projections. See Figures 1 and 2 for locations.

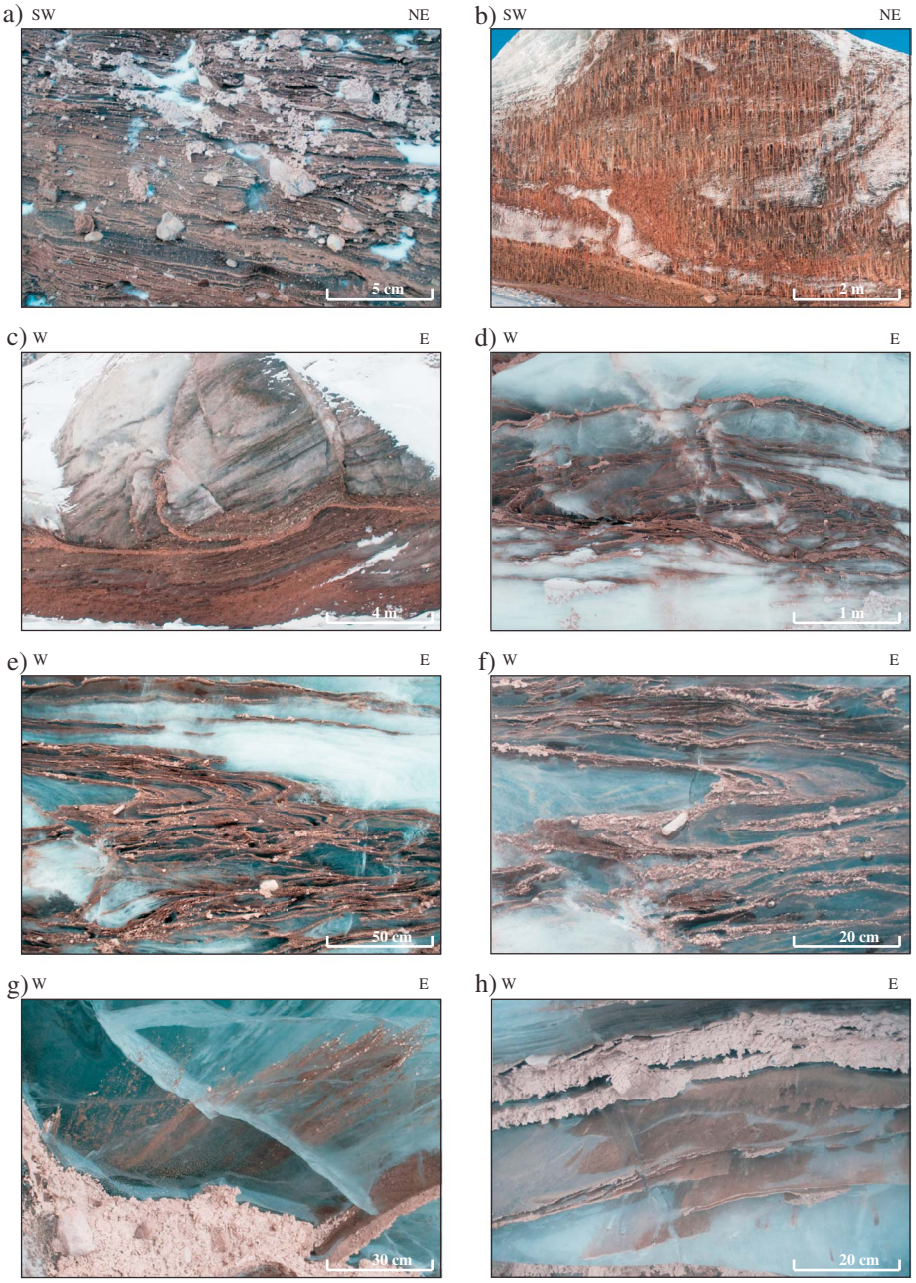

Figure 7. Field photographs of typical structures present within the basal ice. (a) Banded debris-rich ice facies from which most of the samples were collected showing subhorizontal alternating bands (>1–10 mm) of debris-rich and debris-poor ice. (b) Thick (8 m) section of basal ice at NW section with lenses of clean bubbly (englacial) ice. The basal ice is partially obscured by icicles. (c) Banded and solid debris-rich basal ice facies thrust over blocks of clean englacial ice. (d) Folded banded ice showing a double vergence pattern in the folds. (e) Isoclinal recumbent folds verging to the right. (f) Close up of isoclinal "Z" fold showing vergence to the right. The fold axis can be traced through the ice giving a three-dimensional view of the fold. (g) Mineral stretching lineations in debris-poor basal ice above debris-rich horizon. (h) Mineral stretching lineations and elongated bubbles on the surface of debris-rich horizons within clean ice.

For example, the saturation magnetization of hematite is near 3 T while magnetite is fully saturated by 300 mT. The IRM acquisition curves all fail to show complete saturation at 2.5 T indicating the presence of a high-coercivity phase, presumably hematite.

5.2. Anisotropy of Magnetic Susceptibility

[28] Samples yield susceptibility ellipsoids that are predominantly triaxial (Figure 4), where F is roughly equal to L, although variation exists between subsamples, ranging from strongly oblate to strongly prolate (possibly in part

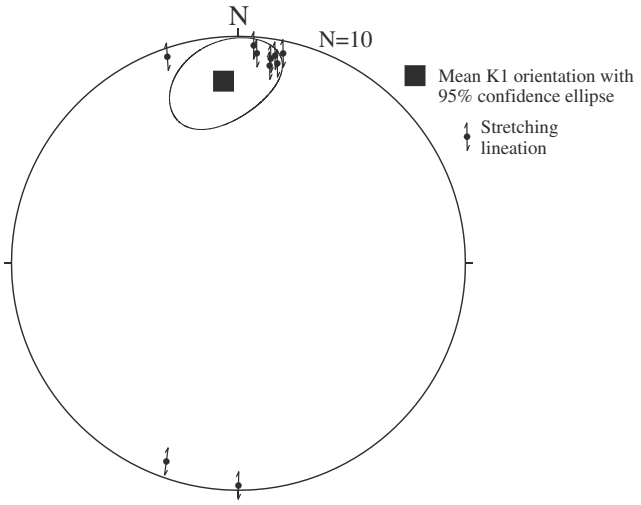

Figure 8. Mineral stretching lineations and mean K_1 orientation with confidence ellipse for SE exposure with 95% confidence ellipses.

arising from the high error margins when calculating parameters at low susceptibilities) [*Biedermann et al*., 2013; *Hrouda*, 2004]. The mean corrected anisotropy degree (P_j) is relatively high (1.05) (Figure 4a) compared with the typical values within sediments dominated by paramagnetic minerals. However, hematite can have very high (>100) anisotropies [*Guerrero-Suarez and Martín-Hernández*, 2012; *Tarling and Hrouda*, 1993] and this high value may reflect the presence of a minor amount of hematite contributing to the anisotropy.

[29] AMS results are shown on lower hemisphere, equal-area stereographic projections (Figure 5) and the corresponding AMS results from individual sites and their sampled locations are shown in Figure 6. The mean maximum susceptibility orientation (K_1) plunges gently (20°) to the north, with a general north-south trend (mean = 359°) (Figure 5), subparallel to dominant glacier flow direction, calculated from the trend of the glacier and orientation of the macroscopic longitudinal foliation. The minimum susceptibility axes (K_3) are subvertical, defining the pole to the magnetic foliation (K_1-K_2 plane). At the NW section (close to the western margin of the glacier), K_1 axes cluster at 20° to 001° and K_3 axes cluster at 030° to 188°. The SE section, despite being close to the opposite margin of the glacier, gives a broadly similar fabric orientation to the SE section with K_1 axes clustering at 20° to 355° and K_3 axes clustering at 27° to 097°.

5.3. Analysis of Visible Structures

[30] In subglacial sediments investigated at other sites, the orientation of magnetic fabrics has been shown to reflect glacier-induced simple shear relating to the flow direction of glacier ice [e.g., *Fleming et al*., 2013; *Hooyer et al*., 2008; *Iverson et al*., 2008; *Shumway and Iverson*, 2009; *Thomason and Iverson*, 2009]. Basal ice lies at this crucial boundary between the bulk glacier ice and deforming bed and, as such, has been interpreted to deform similarly in a way strongly related to the flow of the glacier [*Knight*, 1997]. Evidence for deformation is seen at both sections as a variety of structures including folds, faults, and lineations (Figure 7). One of the unique features of the study of deformation within glacier ice is that, as opposed to most other geological materials, ice is often translucent or transparent. This allows structures to be seen in three dimensions through the ice face (e.g., Figures 7f–7h), aiding analysis and interpretation. These structures can be analyzed to provide insight into the kinematics of deformation, thus providing independent verification of the state of strain within the basal ice. As such, comparisons can be made with the magnetic fabric to determine its relationship to strain within the ice.

[31] Folding and boudinage are common within the basal ice at both sections, especially at the SE section. Here the banded ice facies (Figure 7a), which presumably formed at an orientation parallel to the glacier bed or overriding obstacles, is highly folded in places (Figures 7d–7f). Folds are typically steeply inclined to recumbent and strongly asymmetric, with interlimb angles ranging from tight to isoclinal. One interesting and, at first somewhat confusing, aspect of these folds is that vergence direction can appear on the two-dimensional ice face (Figure 7d) to be in both directions. Folds also occasionally form concentric augen-like rings (Figure 9a). The axes of these folds lie in a north-south orientation, generally parallel to the glacier flow direction and parallel to the maximum susceptibility orientations (K_1). This indicates that rather than being purely cylindrical, which is often assumed, folds are highly noncylindrical in a style often referred to as sheath folding [*Alsop and Carreras*, 2007; *Alsop and Holdsworth*, 2004; *Alsop et al*., 2007].

[32] The fabric of the debris and bubbles within the banded ice facies is not planar. In contrast, a strong linear component is present (Figures 7g and 7h). Debris is observed to be arranged in linear aggregates and has, in places, been strongly smeared along an axis. Lineations, measured at the SW section, cluster at 10° to 005° (Figure 8). In places, strongly elongated bubbles are orientated in the same direction as the debris lineations (Figure 7h). Debris lineations are also seen to form generally parallel to fold axes and almost completely parallel to the magnetic lineation which, in most previous studies of AMS of deformed sediments, represents the direction of stretching [e.g., *Cifelli et al*., 2005; *Liss et al*., 2002; *Parés and van der Pluijm*, 2002].

[33] Faulting is common, illustrating that as well as ductile folding, brittle deformation has also occurred within the basal ice at both sections (Figures 7b and 7c). The NW section contains a number of faults that are typically orientated N-S to NE-SW, shallow to moderately dipping to the east, parallel or subparallel to the glacier margins. At the SE section, faults strike in an N-S orientation; however, both dip angle and dip direction are variable. The majority of the faults have a reverse offset, but many contain subhorizontal debris lineations on their surface, indicating oblique or even transverse slip in some cases and suggesting a transpressional glaciotectonic regime. Thrusting has clearly resulted in the tectonic thickening of basal ice, for example, Figure 7c where banded debris-rich ice has been thrust up over blocks of clean englacial ice.

6. Discussion

6.1. Control on AMS Fabric

[34] The low susceptibility of the samples indicates a volumetrically significant proportion of diamagnetic minerals, presumably quartz, calcite, and ice. Yet, the presence of paramagnetic and ferromagnetic phases provides a positive

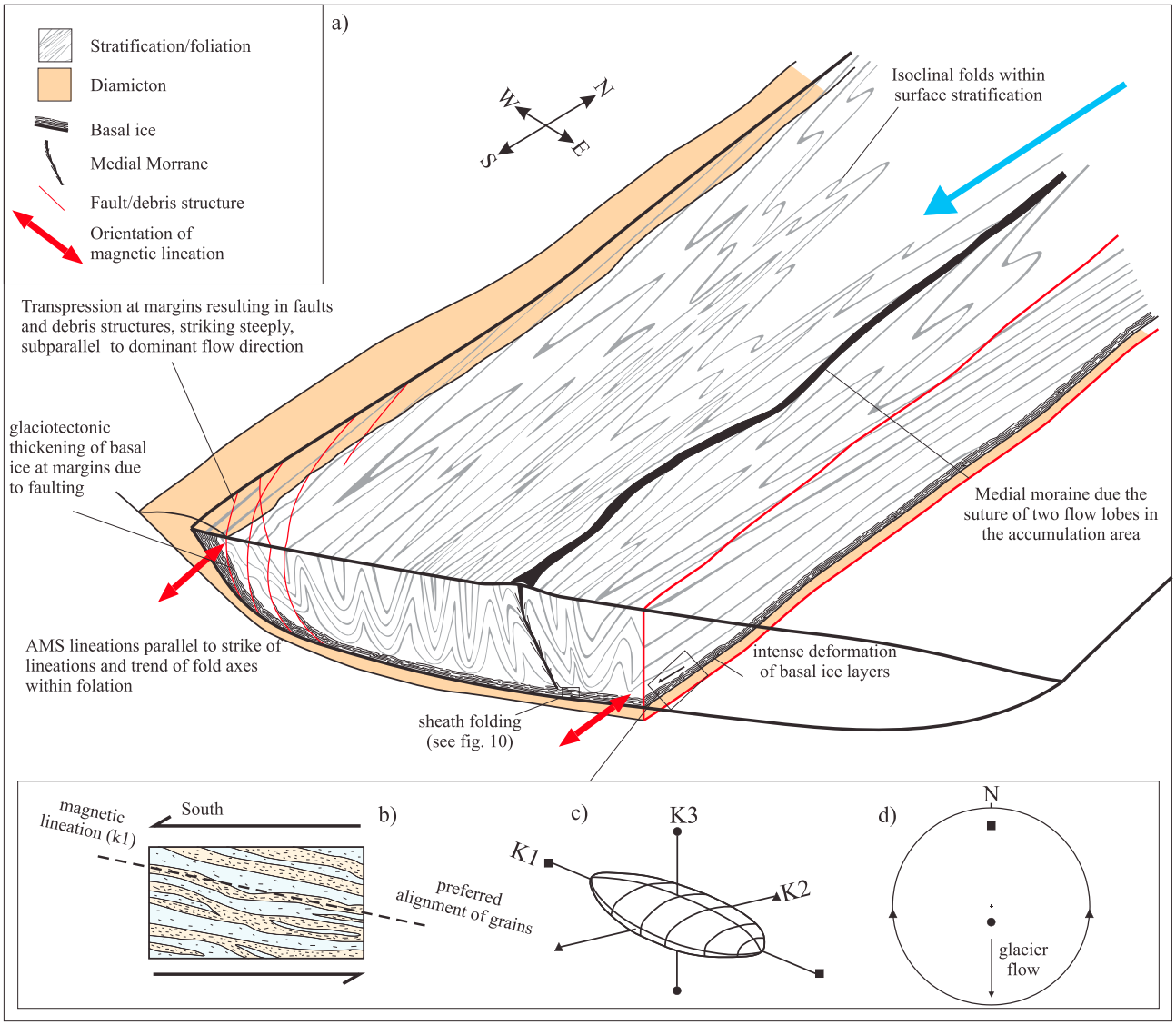

Figure 9. Schematic diagram illustrating the relationship of structures to AMS fabrics. (a) Three-dimensional cartoon of Tunabreen (vertical scale exaggerated) showing the structure of the foliation/stratification, faults, and basal ice in relation to the orientation of the AMS lineation. (b) Sketch of banded basal ice showing the preferred alignment of grains. (c) Visualization of subsequent AMS fabric through the AMS ellipsoid with K_1 (maximum), K_2 (intermediate), and K_3 (minimum) susceptibility axes. (d) Presentation of ellipse through stereonet displaying the mean northerly orientated K_1 parallel to glacier flow direction.

susceptibility which probably controls the magnetic fabric [*Tarling and Hrouda*, 1993]. The dependence of susceptibility on temperature follows Curie-Weiss behavior at low temperatures, suggesting a dominance of paramagnetic minerals [*Richter and van der Pluijm*, 1994]. At high temperatures, the increase in susceptibility can be attributed to the growth of new ferromagnetic minerals with the peak at 550°C, possibly representing a suppressed "Hopkinson peak" of a minor ferromagnetic contribution. The dependence of the susceptibility on field strength could be attributed to a ferromagnetic contribution, since pure paramagnetic minerals yield field-independent behavior [*Hrouda et al.*, 2006], but given the low susceptibility and the strong dependence of susceptibility with temperature, its influence on the AMS is considered minor. The high coercivity picked out by the IRM experiments indicates that hematite most likely controls this ferromagnetic contribution. Therefore, we interpret the origin of the AMS signal as having a mixed magnetic mineralogy. This is dominated by paramagnetic phases which, given the composition of the material, are likely to be phyllosilicate clays with possibly a minor contribution of a high-coercivity ferromagnetic phase, presumably hematite.

[35] The presence of flow-parallel magnetic lineations associated with sediment dominated by phyllosilicate clay minerals and hematite may at first seem counterintuitive as both minerals typically display crystalline anisotropy, where the maximum susceptibility axis lies in the basal plane of the mineral [*Tarling and Hrouda*, 1993]. As such, K_1 orientations are not parallel to the long axis of grains but rather depend on the crystallographic structure with the minimum susceptibility perpendicular to the basal plane. In spite of this, magnetic lineations are common in rocks dominated

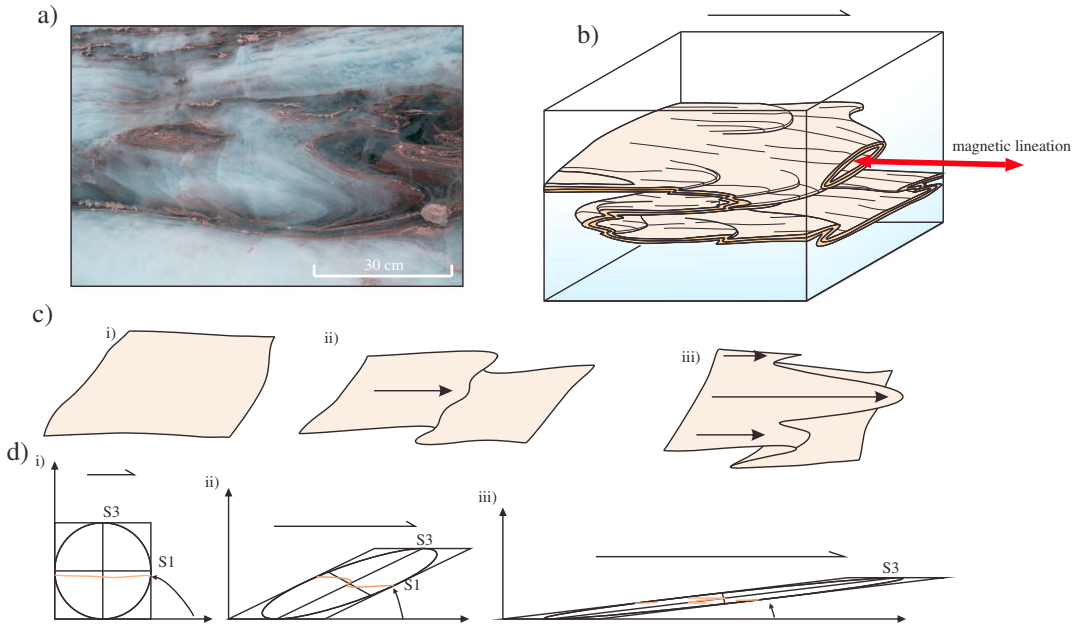

Figure 10. (a) Photograph of sheath fold within banded ice facies from SE section showing augen pattern with concentric rings and double verging folds. (b) Three-dimensional model of sheath folding observed at SE section. (c) Interpretation of sheath fold development and associated strain ellipse, showing (i) predeformation and original configuration, (ii) initial folding, and (iii) evolved sheath folding and rotation of fold axes parallel to flow.

by phyllosilicate minerals and are shown to form parallel to the direction of stretching [*Cifelli et al*., 2005, 2009; *Parés and van der Pluijm*, 2002]. Phyllosilicate minerals tend to break along their basal plane, which when under extensional stresses, become disposed about an axis parallel to stretching, thus creating a magnetic lineation that is directly compatible with fabrics created through shape anisotropy.

6.2. Relationship of Structures to AMS

[36] The magnetic fabrics show strong apparent correspondence with the orientations of macroscopic structures present within the ice. The stratification (mapped in Figure 1 and schematically drawn in Figure 9), which would have originally formed in an orientation parallel to flow boundaries in the accumulation zone, has been tightly folded forming a longitudinal foliation (Figure 9a) under a strong extensional regime. This foliation generally lies parallel to the AMS lineation. The close relationship of the strike of the longitudinal foliation and the AMS lineation within the basal ice suggests that, as one would expect, the basal ice has been deformed by glacier motion.

[37] At the outcrop scale, the banded ice facies within the basal ice have been folded under noncoaxial stretching and simple shear (Figure 10d). In these conditions, folding initiates during the initial stage of shear where the field of compression occurs at a high angle to bedding (Figure 9dii). As deformation continues, the strain ellipse rotates to a low angle to bedding and extensional processes become dominant, resulting in boudinage (Figure 10diii). The folds created within the basal ice at Tunabreen have fold axes which are strongly curvilinear (Figure 9a). This represents a noncylindrical style of folding, commonly referred to as sheath folding [*Alsop et al*., 2007]. Sheath folds normally form when perturbations during the initial stages of folding are greatly exaggerated in high-strain conditions [*Cobbold and Quinquis*, 1980]. As folding progresses, fold noses become stretched and elongated, and fold axes rotate toward the direction of shear within the ice and the fold axes becomes parallel with the main stretching direction (Figure 10c). Sections perpendicular to the shearing direction are characterized by concentric, eye-shaped folds and doubly verging fold directions (Figure 10b). Sheath fold noses lie parallel to the orientation of AMS lineations as fold axes are essentially indistinct from stretching lineations.

[38] Deformation of the ice at Tunabreen has also resulted in the formation of distinct linear features within the basal ice (Figures 7g and 7h). Clusters of debris are smeared out and aligned about an axis. The smearing of grains in basal ice has been referred to in the past [*Hubbard and Sharp*, 1995; *Hubbard et al*., 2000], but its relationship to cumulative strain has not. Similar lineations are often seen in structurally deformed metamorphic rocks [*Neves et al*., 2005; *Twiss and Moores*, 1992], commonly referred to as stretching lineations. Stretching lineations in deformed rocks form in an orientation parallel to the direction of stretching during ductile deformation [*Ramsay and Huber*, 1983]. Thus, structural analysis of their orientation can provide useful information about the kinematics of deformation and deformational history.

[39] At Tunabreen, these lineations lie at an orientation parallel to the fold axes of sheath folds and the strike of macroscopic surface lineations, and subparallel to the flow direction of the glacier. Also, these lineations lie almost completely parallel to the magnetic lineations (Figure 8), thus providing independent verification that these form in an orientation parallel to stretching, and as such, we interpret them as stretching lineations. Under high-strain conditions, detrital grains within

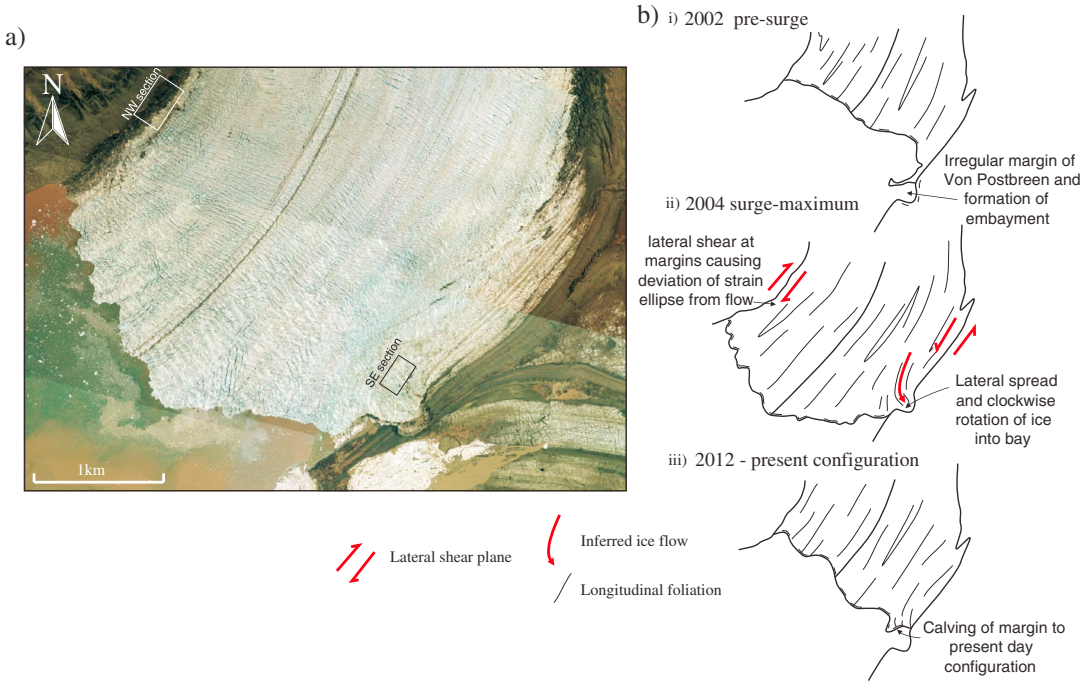

Figure 11. (a) Aerial photograph mosaic of the Tunabreen terminus at surge maximum in 2004 with the location of the sections studied. (b) Interpretation of the formation of the magnetic lineations showing (i) 2002 presurge configuration and irregular margin of Von Postbreen. (ii) 2004 surge maximum showing the orientations of shear in the NW section and the lateral spreading and clockwise rotation of surface foliation and magnetic lineation at the SE section. (iii) Present configuration of Tunabreen at time of study (2012).

the ice will rotate into the most stable orientation about an axis parallel to stretching, forming the lineations. As these lineations are parallel to the interpreted direction of stretching, they can be used in a similar way to which they are in structural geology and the analysis of tectonically deformed rocks in order to give the kinematics of deformation within the ice.

6.3. Kinematics of Deformation Within the Basal Ice

[40] The up-glacier dip of K_1 is a feature commonly seen within subglacial sediments under simple shear [*Shumway and Iverson*, 2009; *Thomason and Iverson*, 2009]. The mean plunge of the K_1 lineation at 20° up glacier may (shown in Figure 5 and drawn schematically in Figures 9b–9d) indicate that within the basal ice, as well as pure shear, there is a component of noncoaxial strain and simple shear causing the updip rotation of K_1 orientations, matching the strain ellipse. Ring shear experiments of subglacial tills subject to simple shear reveal that steady state AMS fabrics develop at strains of 7–30, in which K_1 lies parallel to shear direction dipping 28° away from shear direction [*Hooyer et al.*, 2008; *Iverson et al.*, 2008]. These experiments produced almost identical fabric characteristics and clustering patterns as those displayed in Figure 5. One could argue a similar model for the rotation of grains within basal ice, where slip between the grains and the ice keeps particles from rotating through the shear plane (as suggested by *March* [1932]) therefore rejecting Jeffery rotation [*Jeffery*, 1922] within ice. However, as the magnetic mineralogy of the tills used are different, caution is applied when making direct comparisons, and conclusions should not be made until further laboratory testing on materials with a similar mineralogy is obtained.

6.4. Relationship to Surge Dynamics

[41] At the NW section (Figure 11a), magnetic lineations lie in an orientation that deviates slightly away from the dominant glacier flow direction in this area. If the fabrics formed purely by stretching and shear due to friction at the bed, one may expect the magnetic lineations to trend parallel to ice flow. However, the flow of the glacier ice is not uniform across the ice surface. At the margins, lateral drag can result in the development of marginal shear zones such as those recorded after the 1982–1983 surge of Variegated Glacier [*Lawson et al.*, 1994; *Sharp et al.*, 1988]. At Tunabreen, the deviation of the magnetic lineations from parallel to glacier flow is probably caused by the rotation of the strain ellipse away from glacier flow direction at the margins under noncoaxial strain (Figure 11bi).

[42] At the SE section (Figure 11a), the orientation of the magnetic lineations cannot be explained in the same way, since lateral shear would cause the inclination of lineations in the opposite direction to that observed. However, magnetic lineations lie parallel to longitudinal foliation identified on aerial photographs at that location, indicating that ice flow has been rotated in the opposite direction to that expected. This can be explained by the presence of an irregular presurge carving margin (Figure 10bi). During the surge, local splaying into an embayment facilitated rotation of the ice in an anticlockwise direction (Figure 10bii), causing the slight deviation

from overall flow direction of both the AMS fabrics and surface foliation (Figure 10biii).

6.5. The Use of AMS for the Analysis of Deformation Within Basal Ice

[43] This study has shown that the detrital component of basal ice contains sediment from which an AMS fabric can be measured and provide insight into subglacial processes. The magnetic fabric appears to be a direct reflection of the petrofabric of the detrital grains within the ice. A magnetic lineation is recorded, parallel to the inferred direction of stretching and simple shear within the ice. This result provides support for the validity of the AMS of subglacial sediment, where magnetic lineations are also seen to form parallel to stretching/shear direction within the sediment [*Fleming et al*., 2013; *Gentoso et al*., 2012; *Shumway and Iverson*, 2009; *Thomason and Iverson*, 2009]. The potential preservation of AMS fabrics from basal ice to sediment during melt-out requires further study. However, as an AMS fabric is seen within basal ice, caution should be taken when interpreting AMS fabrics in subglacial sediments as being formed solely by bed deformation, especially when an origin through melt-out is suspected.

[44] Utilizing the methodology described here, the AMS technique can be directly reproduced and applied to other glaciers. AMS has several advantages over other petrofabric techniques [*Iverson et al*., 2008]. The fabric can be determined relatively quickly, accurately, and objectively, and the susceptibility ellipsoid can be calculated in three dimensions. AMS represents the volume average of many grains in each subsample and many subsamples make up a site. Being sensitive to minor changes in the state of strain, investigations of the AMS of basal ice has the potential to provide knowledge on the processes occurring at the ice-bed interface, bridging the gap between the analysis of visible structures at the surface of the glacier and deformation within subglacial sediments. AMS, therefore, has the potential to contribute to the highly debated topic of glacier bed deformation.

[45] AMS has been used to calculate shear strains in deformed rocks and sediment [*Borradaile*, 1988, 1991]. The link between the AMS fabric strength (based on the degree of clustering of susceptibility axes) and strain has also been investigated within subglacial sediments through experimental work with ring shear devices [*Iverson et al*., 2008]. This study showed that fabric strength increases with increasing shear strain, up to a point under which steady state fabrics were reached. In the future, it may be possible to apply similar experimental tests to the AMS of basal ice and thus investigate the link between fabric strength and strain. Also, in contrast to ice-crystal fabric studies, which measure the *c* axis orientation of ice crystals [e.g., *Bader*, 1951; *Tison et al*., 1994; *Wilson and Peternell*, 2011], the AMS fabric is dominated by the paramagnetic and ferromagnetic proportion of detrital material in the basal ice. Therefore, the study of AMS in conjunction with ice-crystal fabric analysis allows the detrital portion of the ice to also be analyzed which, in contrast to glacier ice, is not subject to recrystallization under the pressure/temperature ranges encountered in glaciers.

[46] At this study site, although AMS has highlighted interesting variation in the state of strain, the glacier flow direction was never in a doubt. The site was chosen intentionally as visible structures such as the surface longitudinal foliation measured from aerial photographs and the orientations of folds and lineations at the outcrop scale provide a reference frame for comparison with the AMS results. This has enabled further interpretations to be made and shows that folding style is dominated by sheath folds and lineations which form parallel to stretching within the ice. However, one interesting situation in which AMS could be applied is where the flow direction or past strain history is not known or is poorly understood. For example, on large ice sheets where glacier flow is slow and surface structures are absent or where flow direction is ambiguous [e.g., *Conway et al*., 2002], AMS of basal ice collected from ice cores could potentially be analyzed to provide insight into shear direction at the base of the ice sheet. The AMS technique could also aid research into the subject of massive ground ice, which is thought to originate as the basal portion of pre-existing glaciers often dating back to the Pleistocene, and is often buried and preserved in permafrost regions [*Fritz et al*., 2011; *Waller et al*., 2009]. Here little is known about paleoice flow directions, and therefore, AMS could potentially provide considerable paleoglaciological insight.

7. Conclusions

[47] The AMS fabrics of basal ice and their relationship to deformation during the most recent surge of Tunabreen have been investigated and number of conclusions can subsequently be drawn:

[48] 1. The AMS of basal ice can be measured, and the three components of the susceptibility ellipsoid can rapidly calculated, in the same way that is commonly done for sediment and rock.

[49] 2. Magnetic fabrics at the sections examined are controlled predominantly by the preferred alignment of inclusions of detrital sediment within the ice. The susceptibility and anisotropy in this sediment is dominated by paramagnetic minerals (presumably phyllosilicate clays). In some samples, a high-coercivity phase, presumably hematite is also present, possibly contributing to the fabric.

[50] 3. The folding style within the deformed basal ice is highly noncylindrical. This is not unusual given the high shear strains expected within the deforming ice and the perturbations in flow that exist across the glacier profile. Within subglacial glaciotectonites, since the deformation of underlying subglacial sediments is largely controlled by the overlying ice motion, noncylindrical folding should be expected.

[51] 4. AMS lineations are parallel to, and independently verified by, the macroscopic lineation given by the presence of stretching lineations and the axes of sheath folds. The orientation of stretching lineations in basal ice has the potential to be used as a proxy for stretching direction within the strain ellipse, in the same way that is used in structural geology.

[52] 5. Magnetic lineations at the NW section have been affected by lateral shear, causing a minor amount of deviation of the lineations away from being parallel to the mean trend of the macroscopic foliation, reflecting this noncoaxial deformation. At the SE section, the irregular presurge configuration of the contact between Tunabreen and Von Postbreen has affected strain patterns and led to the anticlockwise rotation of magnetic lineations, stretching lineations, and the macroscopic foliation, resulting in a magnetic lineation orientated subparallel to the dominant glacier flow direction.

[53] **Acknowledgments.** This work forms part of the NERC-funded GAINS (Glacial Activity in Neoproterozoic Svalbard) grant (NE/H004963/1) with a tied PhD studentship held by E.J.F. H.L. was also funded by a NERC PhD studentship (NE/I528050/1). Additional funding for fieldwork was provided by the Queen Mary Postgraduate Research Fund and the Research Council of Norway Arctic Field Grant program. ASTER satellite images were acquired from the NASA Land Processes Distributed Active Archive Center (LPDAAC) and aerial photographs were provided by the NERC Earth Observation Data Centre (NEODC). We would like to thank Bryn Hubbard for his help with the classification of the basal ice facies encountered, the logistical staff at UNIS for their help in the collection of ice cores and preparation (Gerd Irene Sigernes, Martin Indreiten, and Monica Votvik), the other students on the UNIS AG-325 Glaciology course who were also present during the initial inspection of the sections in 2011 and Kathrin Naegeli and Philipp Schuppli for their assistance in the 2012 season. Finally, we would like to thank the two reviewers, Neal Iverson and Peter Knight, for their comments and suggestions and Jeremy Bassis for his editorial assistance.

References

Alsop, G. I., and J. Carreras (2007), The structural evolution of sheath folds: A case study from Cap de Creus, *J. Struct. Geol.*, *29*(12), 1915–1930, doi:10.1016/j.jsg.2007.09.010.

Alsop, G. I., and R. E. Holdsworth (2004), The geometry and topology of natural sheath folds: A new tool for structural analysis, *J. Struct. Geol.*, *26*(9), 1561–1589, doi:10.1016/j.jsg.2004.01.009.

Alsop, G. I., R. E. Holdsworth, and K. J. W. McCaffrey (2007), Scale invariant sheath folds in salt, sediments and shear zones, *J. Struct. Geol.*, *29*(10), 1585–1604, doi:10.1016/j.jsg.2007.07.012.

Bader, H. (1951), Introduction to ice petrofabrics, *The Journal of Geology*, *59*(6), 519–536.

Bamber, J. (1987), Internal reflecting horizons in Spitsbergen glaciers, *Ann. Glaciol.*, *9*, 5–10.

Benn, D. I., and D. J. A. Evans (2010), *Glaciers and Glaciation*, 2nd ed., 816 pp., Hodder Education.

Biedermann, A. R., W. Lowrie, and A. M. Hirt (2013), A method for improving the measurement of low-field magnetic susceptibility anisotropy in weak samples, *J. Appl. Geophys.*, *88*(0), 122–130, doi:10.1016/j.jappgeo.2012.10.008.

Borradaile, G. J. (1988), Magnetic susceptibility, petrofabrics and strain, *Tectonophysics*, *156*(1-2), 1–20, doi:10.1016/0040-1951(88)90279-X.

Borradaile, G. J. (1991), Correlation of strain with anisotropy of magnetic susceptibility (AMS), *PAGEOPH*, *135*(1), 15–29, doi:10.1007/bf00877006.

Borradaile, G. J., and M. Jackson (Eds.) (2004), *Anisotropy of Magnetic Susceptibility (AMS): Magnetic Petrofabrics of Deformed Rocks*, 299–360 pp., Geological Society, London, Special Publications, doi:10.1144/GSL.SP.2004.238.01.18.

Borradaile, G. J., B. S. G. Almqvist, and I. Geneviciene (2012), Anisotropy of magnetic susceptibility (AMS) and diamagnetic fabrics in the Durness Limestone, NW Scotland, *J. Struct. Geol.*, *34*(0), 54–60, doi:10.1016/j.jsg.2011.10.008.

Callot, J. P., P. Robion, W. Sassi, M. L. E. Guiton, J. L. Faure, J. M. Daniel, J. M. Mengus, and J. Schmitz (2010), Magnetic characterisation of folded aeolian sandstones: Interpretation of magnetic fabrics in diamagnetic rocks, *Tectonophysics*, *495*(3–4), 230–245, doi:10.1016/j.tecto.2010.09.020.

Castelnau, O., H. Shoji, A. Mangeney, H. Milsch, P. Duval, A. Miyamoto, K. Kawada, and O. Watanabe (1998), Anisotropic behavior of GRIP ices and flow in Central Greenland, *Earth Planet. Sci. Lett.*, *154*(1–4), 307–322, doi:10.1016/S0012-821X(97)00193-3.

Cifelli, F., M. Mattei, M. Chadima, A. M. Hirt, and A. Hansen (2005), The origin of tectonic lineation in extensional basins: Combined neutron texture and magnetic analyses on "undeformed" clays, *Earth Planet. Sci. Lett.*, *235*(1–2), 62–78, doi:10.1016/j.epsl.2005.02.042.

Cifelli, F., M. Mattei, M. Chadima, S. Lenser, and A. M. Hirt (2009), The magnetic fabric in "undeformed clays": AMS and neutron texture analyses from the Rif Chain (Morocco), *Tectonophysics*, *466*(1–2), 79–88, doi:10.1016/j.tecto.2008.08.008.

Cobbold, P. R., and H. Quinquis (1980), Development of sheath folds in shear regimes, *J. Struct. Geol.*, *2*(1–2), 119–126, doi:10.1016/0191-8141(80)90041-3.

Conway, H., G. Catania, C. Raymond, A. Gades, T. Scambos, and H. Engelhardt (2002), Switch of flow direction in an Antarctic ice stream, *Nature*, *419*(6906), 465–467, doi:10.1038/nature01081.

Cook, S. J., R. I. Waller, and P. G. Knight (2006), Glaciohydraulic supercooling: The process and its significance, *Prog. Phys. Geogr.*, *30*(5), 577–588, doi:10.1177/0309133306071141.

Cutbill, J. L., and A. Challinor (1965), Revision of the stratigraphical scheme for the carboniferous and permian rocks of Spitsbergen and Bjørnøya, *Geol. Mag.*, *102*(05), 418–439, doi:10.1017/S0016756800053693.

Dallmann, W. K., K. Piepjohn, D. Blomeier, and S. Elvevold (2009), Geological map of Svalbard 1:100,000, sheet C8G Billefjorden, Norsk Polarinstitutt, Tromsø.

Dallmann, W. K., K. Piepjohn, G. P. Halverson, S. Elvevold, and D. Blomeier (2011), Geological map Svalbard 1:100 000, sheet D6G Vaigattbogen, Norsk Polarinstitutt, Tromsø.

de Wall, H., M. Bestmann, and K. Ullemeyer (2000), Anisotropy of diamagnetic susceptibility in Thassos marble: A comparison between measured and modeled data, *J. Struct. Geol.*, *22*(11–12), 1761–1771, doi:10.1016/S0191-8141(00)00105-X.

Dunlop, D. J., and O. Özdemir (1997), *Rock Magnetism: Fundamentals and Frontiers*, 596 pp., Cambridge Univ. Press, Cambridge.

Ellwood, B. B., and M. T. Ledbetter (1977), Antarctic bottom water fluctuations in the Vema Channel: Effects of velocity changes on particle alignment and size, *Earth Planet. Sci. Lett.*, *35*(2), 189–198, doi:10.1016/0012-821X(77)90121-2.

Evans, D. J. A., and D. I. Benn (2004), *A Practical Guide to the Study of Glacial Sediments*, 266 pp., Arnold London, London.

Eyles, N., T. E. Day, and A. Gavican (1987), Depositional controls on the magnetic characteristics of lodgement tills and other glacial diamict facies, *Can. J. Earth Sci.*, *34*, 2436–2458.

Ferré, E. C. (2002), Theoretical models of intermediate and inverse AMS fabrics, *Geophys. Res. Lett.*, *29*(7), 31–31, doi:10.1029/2001GL014367.

Fleming, E. J., C. T. E. Stevenson, and M. S. Petronis (2013), New insights into the deformation of a Middle Pleistocene glaciotectonised sequence in Norfolk, England through magnetic and structural analysis, *Proc. Geol. Assoc.*, *124*, doi:10.1016/j.pgeola.2012.11.004, in press.

Fritz, M., S. Wetterich, H. Meyer, L. Schirrmeister, H. Lantuit, and W. H. Pollard (2011), Origin and characteristics of massive ground ice on Herschel Island (western Canadian Arctic) as revealed by stable water isotope and hydrochemical signatures, *Permafrost and Periglacial Processes*, *22*(1), 26–38, doi:10.1002/ppp.714.

Gentoso, M. J., E. B. Evenson, K. P. Kodama, N. R. Iverson, R. B. Alley, C. Berti, and A. Kozlowski (2012), Exploring till bed kinematics using AMS magnetic fabrics and pebble fabrics: The Weedsport drumlin field, New York State, USA, *Boreas*, *41*(1), 31–41, doi:10.1111/j.1502-3885.2011.00221.x.

Guerrero-Suarez, S., and F. Martín-Hernández (2012), Magnetic anisotropy of hematite natural crystals: Increasing low-field strength experiments, *Int. J. Earth Sci.*, *101*(3), 625–636, doi:10.1007/s00531-011-0666-y.

Hambrey, M. J., and N. F. Glasser (2003), The role of folding and foliation development in the genesis of medial moraines: Examples from Svalbard glaciers, *The Journal of Geology*, *111*(4), 471–485.

Hambrey, M. J., and W. Lawson (Eds.) (2000), *Structural Styles and Deformation Fields in Glaciers: A Review*, 59–83 pp., Geological Society London Special Publications, doi:10.1144/GSL.SP.2000.176.01.06.

Hambrey, M. J., T. Murray, N. F. Glasser, A. Hubbard, B. Hubbard, G. Stuart, S. Hansen, and J. Kohler (2005), Structure and changing dynamics of a polythermal valley glacier on a centennial timescale: Midre Lovénbreen, Svalbard, *J. Geophys. Res.*, *110*, F01006, doi:10.1029/2004JF000128.

Hargraves, R. B., D. Johnson, and C. Y. Chan (1991), Distribution anisotropy: The cause of AMS in igneous rocks?, *Geophys. Res. Lett.*, *18*(12), 2193–2196, doi:10.1029/91GL01777.

Harland, W. B., L. M. Anderson, D. Manasrah, and N. J. Butterfield (1997), *The Geology of Svalbard*, Geological Society Publishing House.

Hodgkins, R., and J. A. Dowdeswell (1994), Tectonic processes in Svalbard tide-water glacier surges: Evidence from structural glaciology, *J. Glaciol.*, *40*(136), 553–560.

Hooyer, T. S., N. R. Iverson, F. Lagroix, and J. F. Thomason (2008), Magnetic fabric of sheared till: A strain indicator for evaluating the bed deformation model of glacier flow, *J. Geophys. Res.*, *113*, F02002, doi:10.1029/2007JF000757.

Hrouda, F. (Ed.) (2004), *Problems in Interpreting AMS Parameters in Diamagnetic Rocks*, 49–59 pp., Geological Society, London, Special Publications, doi:10.1144/gsl.sp.2004.238.01.05.

Hrouda, F., and A. Kapička (1986), The effect of quartz on the magnetic anisotropy of quartzite, *Stud. Geophys. Geod.*, *30*(1), 39–45.

Hrouda, F., M. Chlupácová, and S. Mrázová (2006), Low-field variation of magnetic susceptibility as a tool for magnetic mineralogy of rocks, *Phys. Earth Planet. Inter.*, *154*(3-4), 323–336, doi:10.1016/j.pepi.2005.09.013.

Hubbard, B. (1991), Freezing-rate effects on the physical characteristics of basal ice formed by net adfreezing, *J. Glaciol.*, *37*(127).

Hubbard, B., and M. Sharp (1989), Basal ice formation and deformation: A review, *Prog. Phys. Geogr.*, *13*(4), 529–558, doi:10.1177/030913338901300403.

Hubbard, B., and M. Sharp (1993), Weertman regelation, multiple refreezing events and the isotopic evolution of the basal ice layer, *J. Glaciol.*, *39*(132), 275–291.

Hubbard, B., and M. Sharp (1995), Basal ice facies and their formation in the western Alps, *Arct. Alp. Res.*, *27*, 301–310.

Hubbard, B., J.-L. Tison, L. Janssens, and B. Spiro (2000), Ice-core evidence of the thickness and character of clear-facies basal ice: Glacier de Tsanfleuron, Switzerland, *J. Glaciol.*, *46*(152), 140–150, doi:10.3189/172756500781833250.

Hubbard, B., S. Cook, and H. Coulson (2009), Basal ice facies: A review and unifying approach, *Quat. Sci. Rev.*, *28*(19–20), 1956–1969, doi:10.1016/j.quascirev.2009.03.005.

Iverson, N. R., T. S. Hooyer, J. F. Thomason, M. Graesch, and J. R. Shumway (2008), The experimental basis for interpreting particle and magnetic fabrics of sheared till, *Earth Surf. Processes Landforms*, *33*(4), 627–645, doi:10.1002/esp.1666.

Jeffery, G. B. (1922), The motion of ellipsoidal particles immersed in a viscous fluid, in *Proceedings of the Royal Society of London. Series A, Containing Papers of a Mathematical and Physical Character*, *102*(715), 161-179.

Jelínek, V. (1981), Characterization of the magnetic fabric of rocks, *Tectonophysics*, *79*(3–4), T63–T67, doi:10.1016/0040-1951(81)90110-4.

Khan, M. A. (1962), The anisotropy of magnetic susceptibility of some igneous and metamorphic rocks, *J. Geophys. Res.*, *67*(7), 2873–2885, doi:10.1029/JZ067i007p02873.

Knight, P. G. (1997), The basal ice layer of glaciers and ice sheets, *Quat. Sci. Rev.*, *16*(9), 975–993, doi:10.1016/s0277-3791(97)00033-4.

Lagroix, F., and S. K. Banerjee (2002), Paleowind directions from the magnetic fabric of loess profiles in central Alaska, *Earth Planet. Sci. Lett.*, *195*(1-2), 99–112, doi:10.1016/S0012-821X(01)00564-7.

Lanci, L., D. V. Kent, P. E. Biscaye, and A. Bory (2001), Isothermal remanent magnetization of Greenland ice: Preliminary results, *Geophys. Res. Lett.*, *28*(8), 1639–1642, doi:10.1029/2000GL012594.

Larsen, N. K., C. Kronborg, J. C. Yde, and N. T. Knudsen (2010), Debris entrainment by basal freeze-on and thrusting during the 1995–1998 surge of Kuannersuit Glacier on Disko Island, west Greenland, *Earth Surf. Processes Landforms*, *35*(5), 561–574, doi:10.1002/esp.1945.

Lawson, W. J., M. J. Sharp, and M. J. Hambrey (1994), The structural geology of a surge-type glacier, *J. Struct. Geol.*, *16*(10), 1447–1462, doi:10.1016/0191-8141(94)90008-6.

Liss, D., D. H. W. Hutton, and W. H. Owens (2002), Ropy flow structures: A neglected indicator of magma-flow direction in sills and dikes, *Geology*, *30*(8), 715, doi:10.1130/0091-7613(2002).

Maltman, A. J., B. Hubbard, and M. J. Hambrey (2000), Deformation of glacial materials: Introduction and overview, *Geological Society London Special Publications*, *176*(1), 1, doi:10.1144/GSL.SP.2000.176.01.01.

Mansell, D., A. Luckman, and T. Murray (2012), Dynamics of tidewater surge-type glaciers in northwest Svalbard, *J. Glaciol.*, *58*(207), 110–118, doi:10.3189/2012JoG11J058.

March, A. (1932), Mathematical theory on regulation according to the particle shape and affine deformation, *Z. Kristall.*, *81*(3/4), 285–297.

Murray, T., T. Strozzi, A. Luckman, H. Jiskoot, and P. Christakos (2003), Is there a single surge mechanism? Contrasts in dynamics between glacier surges in Svalbard and other regions, *J. Geophys. Res.*, *108*(B5), 2237, doi:10.1029/2002JB001906.

Nagata, T. (1961), *Rock magnetism*, Maruzen, Tokyo.

Neves, S. P., J. M. R. da Silva, and G. Mariano (2005), Oblique lineations in orthogneisses and supracrustal rocks: Vertical partitioning of strain in a hot crust (eastern Borborema Province, NE Brazil), *J. Struct. Geol.*, *27*(8), 1513–1527, doi:10.1016/j.jsg.2005.02.002.

Owens, W. H., and E. H. Rutter (1978), The development of magnetic susceptibility anisotropy through crystallographic preferred orientation in a calcite rock, *Phys. Earth Planet. Inter.*, *16*(3), 215–222, doi:10.1016/0031-9201(78)90014-6.

Parés, J. M., and B. A. van der Pluijm (2002), Evaluating magnetic lineations (AMS) in deformed rocks, *Tectonophysics*, *350*(4), 283–298, doi:10.1016/S0040-1951(02)00119-1.

Parés, J. M., B. A. van der Pluijm, and J. Dinarès-Turell (1999), Evolution of magnetic fabrics during incipient deformation of mudrocks (Pyrenees, northern Spain), *Tectonophysics*, *307*(1-2), 1–14, doi:10.1016/S0040-1951(99)00115-8.

Ramsay, J. G., and M. I. Huber (1983), *The Techniques of Modern Structural Geology, Volume 1: Strain Analysis*, Academic Press, London.

Richter, C., and B. A. van der Pluijm (1994), Separation of paramagnetic and ferrimagnetic susceptibilities using low temperature magnetic susceptibilities and comparison with high field methods, *Phys. Earth Planet. Inter.*, *82*(2), 113–123, doi:10.1016/0031-9201(94)90084-1.

Rigsby, G. P. (1958), Fabrics of glacier and laboratory deformed ice, paper presented at Symposium on Physics of the Movement of the Ice, Symposium of Chamonix.

Rochette, P. (1987), Magnetic susceptibility of the rock matrix related to magnetic fabric studies, *J. Struct. Geol.*, *9*(8), 1015–1020, doi:10.1016/0191-8141(87)90009-5.

Samyn, D., A. Svensson, and S. J. Fitzsimons (2008), Dynamic implications of discontinuous recrystallization in cold basal ice: Taylor Glacier, Antarctica, *J. Geophys. Res.*, *113*, F03S90, doi:10.1029/2006JF000600.

Samyn, D., S. Fitzsimons, and R. Lorrain (2010), Rotating micro-structures in Antarctic cold basal ice: Implications for glacier flow and its interpretation, *Int. J. Earth Sci.*, *99*(8), 1849–1857, doi:10.1007/s00531-009-0478-5.

Sharp, M., W. Lawson, and R. S. Anderson (1988), Tectonic processes in a surge-type glacier, *J. Struct. Geol.*, *10*(5), 499–515, doi:10.1016/0191-8141(88)90037-5.

Shumway, J. R., and N. R. Iverson (2009), Magnetic fabrics of the Douglas Till of the Superior lobe: Exploring bed-deformation kinematics, *Quat. Sci. Rev.*, *28*(1-2), 107–119, doi:10.1016/j.quascirev.2008.09.020.

Souchez, R., G. Vandenschrick, R. Lorrain, and J. L. Tison (2000), Basal ice formation and deformation in central Greenland: A review of existing and new ice core data, *Geological Society London Special Publications*, *176*(1), 13, doi:10.1144/GSL.SP.2000.176.01.02.

Tarling, D. H., and F. Hrouda (1993), *The Magnetic Anisotropy of Rocks*, 217 pp., Chapman & Hall, London.

Thomason, J. F., and N. R. Iverson (2006), Microfabric and microshear evolution in deformed till, *Quat. Sci. Rev.*, *25*(9-10), 1027–1038.

Thomason, J. F., and N. R. Iverson (2009), Deformation of the Batestown till of the Lake Michigan lobe, Laurentide ice sheet, *J. Glaciol.*, *55*(189), 131–146, doi:10.3189/002214309788608877.

Tison, J. L., and R. Lorrain (1987), A mechanism of basal ice-layer formation involving major ice-fabric changes, *J. Glaciol.*, *33*(113), 47–50.

Tison, J. L., T. Thorsteinsson, R. D. Lorrain, and J. Kipfstuhl (1994), Origin and development of textures and fabrics in basal ice at Summit, Central Greenland, *Earth Planet. Sci. Lett.*, *125*(1–4), 421–437, doi:10.1016/0012-821x(94)90230-5.

Twiss, R. J., and E. M. Moores (1992), *Structural Geology*, 532 pp., WH Freeman, New York.

Waller, R. I., J. B. Murton, and P. G. Knight (2009), Basal glacier ice and massive ground ice: Different scientists, same science?, *Geological Society, London, Special Publications*, *320*(1), 57–69, doi:10.1144/sp320.5.

Wilen, L. A., C. L. Diprinzio, R. B. Alley, and N. Azuma (2003), Development, principles, and applications of automated ice fabric analyzers, *Microsc. Res. Tech.*, *62*(1), 2–18, doi:10.1002/jemt.10380.

Wilson, C. J. L. (2000), Experimental work on the effect of pre-existing anisotropy on fabric development in glaciers, *Geological Society London Special Publications*, *176*(1), 97, doi:10.1144/GSL.SP.2000.176.01.08.

Wilson, C. J. L., and M. Peternell (2011), Evaluating ice fabrics using fabric analyser techniques in Sorsdal Glacier, East Antarctica, *J. Glaciol.*, *57*(205), 881–894, doi:10.3189/002214311798043744.

Wilson, C. J. L., and H. M. Sim (2002), The localization of strain and c-axis evolution in anisotropic ice, *J. Glaciol.*, *48*(163), 601–610, doi:10.3189/172756502781831034.